The role of host phenology for parasite transmission

Hannelore MacDonald[1,*], Erol Akçay[1], Dustin Brisson[1]

1. Department of Biology, University of Pennsylvania, Philadelphia, Pennsylvania 19104;
∗ Corresponding author; e-mail: haime@sas.upenn.edu

Abstract

Phenology is a fundamental determinant of species distributions, abundances, and interactions. In host-parasite interactions, host phenology can affect parasite fitness due to the temporal constraints it imposes on host contact rates. However, it remains unclear how parasite transmission is shaped by the wide range of phenological patterns observed in nature. We develop a mathematical model of the Lyme disease system to study the consequences of differential tick developmental-stage phenology for the transmission of *B. burgdorferi*. Incorporating seasonal tick activity can increase *B. burgdorferi* fitness compared to continuous tick activity but can also prevent transmission completely. Slightly asynchronous tick developmental-stage phenology results in high *B. burgdorferi* fitness compared to synchronous tick activity. Surprisingly, *B. burgdorferi* is eradicated as asynchrony increases further due to feedback from mouse population dynamics. These results highlight the importance of phenology, a ubiquitous driver of species interactions, for the fitness of a parasite.

Introduction

Behaviors or traits that vary seasonally, termed phenology in the ecological literature, impact both the type and strength of ecological interactions within populations and communities.[1–5] For example, seasonally-matching flowering times and pollinator activity periods is a key driver of short- and long-term population dynamics of both plants and insects.[6–11] Differences in the seasonal activities of interacting species over time or geography, caused by changes in climatic and environmental features, can result in population extinctions and in population explosions.[12–18] Although the majority of studies focus on the phenology of plants and their interacting species, the seasonal activity of hosts or disease vectors is likely to also have large impacts on the population dynamics of infectious microbes.

The impact of phenology on disease transmission dynamics can be prominent in disease systems involving multiple host species or life-stages, because the seasonal match or mismatch of activities between species or stages will determine the frequency and type of pathogen transmission. For instance, consider the cestode *Schistocephalus solidus* that infects young three-spined stickleback fish as an intermediate host, multiplies within the fish before the fish is eaten by the definitive bird host (belted kingfisher).[19,20] The parasite reproduces sexually within the bird who defecate parasite eggs that infect juvenile fish.[19] This disease system occurs in North American lakes that freeze over winter, causing both fish reproduction and bird migration to be temporally restricted within each year. A temporal mismatch in the bird and fish phenologies, such as fish reproduction occurring prior to the return migration of birds, could therefore reduce or eliminate cestode transmission among its hosts. Further, variation in the environmental cues affecting the seasonal activity patterns of the birds and fish either among lakes or across years is likely to impact disease transmission dynamics. Seasonal dynamics such as these are expected to impact parasite fitness in many disease systems, yet the quantitative and qualitative impact of phenology remains relatively underexplored.[4]

Human diseases caused by zoonotic pathogens, those that complete their natural life cycle in wildlife but that can infect humans, are likely impacted by the phenology of their wildlife hosts or vectors. Parasites transmitted by hard bodied ticks (family Ixodidae) represent a practical case study for the impact of phenology on disease systems. The public health importance of diseases transmitted by these ticks, such as Lyme disease, has resulted in expansive field datasets that provide baseline expectations for the transmission consequences of tick phenological patterns, making this a good system to study the effects of the general conceptual issue of how vector phenology drives parasite transmission.[21–23] Ixodid ticks have three distinct developmental stages. Larvae, the first developmental stage, hatch uninfected but can acquire *Borrelia burgdorferi*, the etiological agent of Lyme disease, while feeding on an infected host (Fig. 1). Fed larvae molt to nymphs that can then transmit *B. burgdorferi* to small vertebrate hosts (primarily mice, chipmunks, and shrews) during nymphal feeding. Fed nymphs molt to adults that feed on large vertebrates before laying eggs that hatch as larvae. In the Northeastern US, the nymphal stage is active in early summer while larvae from a different cohort feed in late summer, providing an opportunity for the infection to be transmitted from nymphs to larvae through the vertebrate hosts. This sequential feeding pattern has been alleged to contribute to higher infection prevalence in the Northeastern US relative to Southern US or the Midwest, where the sequential activity patterns are less pronounced.[23,24]

Here we develop a model to study the evolutionary ecology of parasite transmission given different phenological scenarios using the *B. burgdorferi* -*Ixodes* tick system as a natural example. Our model is relatively simple, making mathematical analyses tractable while capturing the fundamental impact of phenology on parasite fitness. This impact unfolds over two time-scales: the within-season dynamics of infection, and the between-season demography of the vector.[2] Previous work[25,26] considered the within-season

dynamics of infection but did not account for the between-season population dynamics of the vector species. The latter is an important factor as phenology can alter vector population sizes resulting in an ecological feedback impacting parasite fitness. Our analysis builds on a modeling framework that integrates these effects[2] and demonstrates a general approach for studying both the short- and long-term effects of vector phenology for parasite fitness. We use the Lyme disease system to describe our approach, although the modeling framework applies to all parasites that require multiple transmission events to complete their life cycle (*e.g.* West Nile Virus, Leishmania parasites, *Yersinia pestis*). Our framework can be extended to study how specific vector life history traits, such as differential mortality throughout the year, impact parasite fitness. Additionally, our straightforward framework makes further investigation of the evolutionary pressure imposed by phenology possible.

Model

We model the transmission of *B. burgdorferi* between *I. scapularis* and a main vertebrate reservoir, the white-footed mouse, *Peromyscus leucopus*.[27] Our model tracks the within-season dynamics of nymphal and larval population activity and uses these dynamics to compute the between season changes in overall infection prevalence.

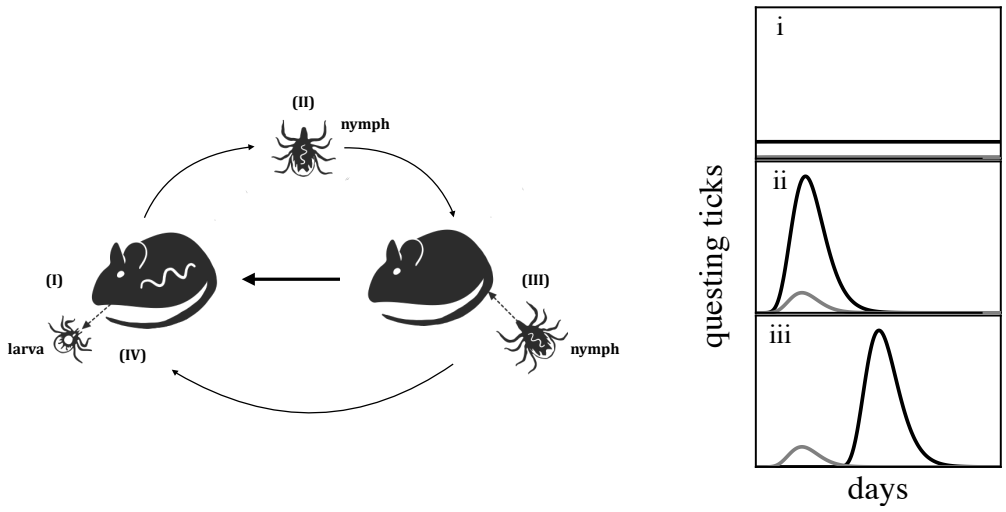

(a) (b)

Figure 1: How does tick life-stage phenology impact the transmission of *B. burgdorferi*? (*a.*) Larval ticks hatch uninfected ([28]) and can acquire *B. burgdorferi* by feeding on an infected small animal (*I*). Infected larvae molt to nymphs and become active the following year (*II*). Small animals are infected when fed upon by an infected nymph (*III*). Fed nymphs molt to adults and feed on larger animals prior to laying eggs that hatch the following year (*IV*). Adult ticks play a minor role in the transmission ecology of *B. burgdorferi* and are thus not explicitly modeled. (*b.*) The seasonal activity patterns of the tick developmental stages vary from near-continuous activity of all stages throughout the year (*i*) ([23]) to developmental stages with temporally divergent activity seasons of short-duration within the US (iii).[23] This latter tick-stage phenology (iii) is thought to result in high transmission of *B. burgdorferi* as large proportions of hosts are infected by nymphs (III) prior to larval activity (I). Note that the larvae and nymphs that feed in the same summer are from different cohorts.

Within-season dynamics describe the duration of nymphal and larval emergence and feeding activity in continuous time from the beginning of each season ($t = 0$) to the end ($t = \tau$). The life-cycle we model is depicted in Figure 1a. Ticks start their life-cycle uninfected, but may pick up the infection as larvae by feeding on an infected mouse. Larvae then overwinter and emerge as nymphs in the next season who can transmit the infection to new mice. The state variables $L_\bullet(t)$, $N_\bullet(t)$, and $M_\bullet(t)$ represent larval, nymphal, and mouse populations, where the subscripts denote whether ticks are questing (q) or fed (f), as well as infection status of ticks and mice (i for infected, u for uninfected). Thus, L_q denotes the questing larvae (who by definition cannot be infected), while L_{if} denotes fed larvae that are infected. The within season dynamics are given by the following system of ordinary differential equations:

$$\frac{dL_q}{dt} = \hat{L}(T)g_l(t,\theta_l) - L_q(\gamma_l(M_i + M_u) + \mu_l), \tag{1a}$$

$$\frac{dL_{if}}{dt} = \beta_{ml}\gamma_l L_q M_i, \tag{1b}$$

$$\frac{dL_{uf}}{dt} = \gamma_l L_q(M_u + (1-\beta_{ml})M_i), \tag{1c}$$

$$\frac{dN_{iq}}{dt} = \hat{N}_i(T)g_n(t,\theta_n) - N_{iq}(\gamma_n(M_i + M_u) + \mu_n), \tag{1d}$$

$$\frac{dN_{uq}}{dt} = \hat{N}_u(T)g_n(t,\theta_n) - N_{uq}(\gamma_n(M_i + M_u) + \mu_n), \tag{1e}$$

$$\frac{dN_f}{dt} = \gamma_n(N_{iq} + N_{uq})(M_i + M_u), \tag{1f}$$

$$\frac{dM_u}{dt} = bM(1-(M)/k) - \mu_m M_u - \beta_{nm}\gamma_n N_{iq} M_u, \tag{1g}$$

$$\frac{dM_i}{dt} = \beta_{nm}\gamma_n N_{iq} M_u - \mu_m M_i\,. \tag{1h}$$

Here, $\hat{L}(T)$ represents the total larval population to emerge in year T, as determined by the number of nymphs that have successfully fed in the previous year, $T-1$, survived to adulthood, and reproduced (given by equation (4) below). Similarly, $\hat{N}_i(T)$ and $\hat{N}_u(T)$ represent the total number of questing infected and uninfected nymphs that emerge in a year T as determined by the number of infected and uninfected larvae at the end of the previous year and the probability of over-winter survival (see equations (2) and (3)). All other parameters are described in the table below.

The functions $g_l(t, l_l)$ and $g_l(t, l_n)$ are probability density functions describing the timing and length of larval and nymphal emergence respectively. We describe tick emergence using a uniform distribution for analytical tractability, but other distributions can be used.

$$g_\bullet(t, l_\bullet) = \begin{cases} 0 & t < t_{\bullet 0} \\ \frac{1}{l_\bullet} & t_{\bullet 0} \le t \le t_{\bullet f} \\ 0 & t_{\bullet f} < \tau \end{cases}$$

Where $t_{\bullet 0}$ is the time emergence begins, $t_{\bullet f}$ is the time emergence stops and $l_\bullet$ is the emergence length ($t_{\bullet 0} + t_{\bullet f} = l_\bullet$)

We solve equations 1a-g analytically, assuming the host population is at equilibrium in Appendix B.

Parameter	Description	Value
$t_{\bullet 0}$	start of activity period for tick life stage $\bullet$	varies
$t_{\bullet f}$	end of emergence period for tick life stage $\bullet$	varies
$l_{\bullet}$	length of emergence period for tick life stage $\bullet$	varies
$\hat{L}$	size of emerging larval population	varies
$\hat{N}_i$	size of emerging infected nymphal population	varies
$\hat{N}_u$	size of emerging uninfected nymphal population	varies
γ_l	density dependent contact rate between larvae and mice	0.004[29]
γ_n	density dependent contact rate between nymphs and mice	0.008[29]
β_{nm}	transmission probability from nymphs to mice	0.83[30]
β_{hm}	transmission probability from mice to larvae	0.6[30]
μ_l	larval death rate	0.006[31]
μ_n	nymphal death rate	0.006[31]
μ_m	mouse death rate	0.01[32]
b	mouse birth rate	0.01[32]
k	mouse carrying capacity	varies[27]
σ_l	larval overwintering survival probabilty	0.4[30]
σ_n	compound fecundity and survival parameter	10[30]
α	density dependence parameter	0.0045

Table 1

Between-season dynamics

The within-season dynamics described above are coupled to recurrence equations that describe the survival of larvae and nymphs between years. The total number of infected and uninfected nymphs ($\hat{N}_i(T+1)$ and $\hat{N}_u(T+1)$) that emerge in a given year are given as a function of the number of infected and uninfected fed larvae at the end of the previous year ($L_{if}(\tau)$ and $L_{uf}(\tau)$) as follows:

$$\hat{N}_i(T+1) = \sigma_l L_{if}(\tau)\,, \tag{2}$$

$$\hat{N}_u(T+1) = \sigma_l L_{uf}(\tau) \tag{3}$$

where $L_{if}(\tau)$ and $L_{uf}(\tau)$ are the infected and uninfected larval abundances at the end of the previous season (see Appendix B) and σ_l is the larval overwintering survival probability.

Similarly, the total fed nymphal population at the end of the year $N_f(\tau)$ gives rise to the population of larvae, $\hat{L}(T+1)$, that emerges the following year as described by the map:

$$\hat{L}(T+1) = \frac{\sigma_n N_f(\tau)}{1+\alpha N_f(\tau)} \tag{4}$$

where $N_f(\tau)$ is found by integrating (1e) over the season from $(0,\,\tau)$ as shown in Appendix B. σ_n is the expected number of eggs produced per fed nymph, after accounting for survival to adulthood and for fecundity. The strength of density dependence on reproduction is determined by α.

With these functions, we can write the discrete, between season mapping of the total larval and nymphal

abundances from one year to the next:

$$\hat{L}(T+1) = \frac{\sigma_n \phi_n \hat{N}(T)}{1 + \alpha \phi_n \hat{N}(T)} , \tag{5}$$

$$\hat{N}_i(T+1) = \sigma_l \phi_{li}(\hat{N}_i(T)) \hat{L}(T) , \tag{6}$$

$$\hat{N}_u(T+1) = \sigma_l \phi_{lu}(\hat{N}_i(T)) \hat{L}(T) \tag{7}$$

where ϕ_n denotes the fraction of emerging nymphs that successfully feed as calculated from within-season dynamics ($\phi_n = \frac{N_f(\tau)}{\hat{N}(T)}$; see Appendix A), and $\phi_{li}(\hat{N}_i(T))$ and $\phi_{lu}(\hat{N}_i(T))$ are functions of $\hat{N}_i(T)$ that denote the fraction of emerging larvae that become infected or remain uninfected through feeding as calculated from within-season dynamics (e.g., $\phi_{li}(\hat{N}_i(T)) = \frac{L_{if}(\tau)}{\hat{L}(T)}$; see Appendix B).

We next calculate the basic reproductive number, R_0, of the parasite to quantify the impact of phenology for *B. burgdorferi* fitness. R_0 represents the average number of new infections caused by a single infected tick in an otherwise naïve population of mammals and ticks,[33] which gives the threshold for parasite invasibility given the phenology of both tick stages. R_0 is computed as the number of infected nymphs that emerge in year $T+1$ produced by a single infected nymph that emerged in year T in an otherwise uninfected population. Specifically, we consider a tick population that is at its demographic equilibrium without the infection, solved by setting $\hat{L}^* = \hat{L}(T)$, $\hat{N}^* = \hat{N}_u(T) - 1$, and $\hat{N}_i(T) = 1$ in equations (5)- (7). At this demographic equilibrium, R_0 of a rare parasite infection is given as follows:

$$R_0 = \frac{\hat{N}_i(T+1)}{\hat{N}_i(T)} = \sigma_l \phi_{li}(\hat{N}_i) \hat{L}^* \tag{8}$$

This R_0 accounts for transmission between cohorts of ticks through intermediate mouse hosts in a given feeding season. When $\hat{N}_i(T) = 1$, parasites persist in phenological scenarios where $\hat{N}_i((T+1)) \geq 1$ (*i.e.* slope is greater than or equal to unity). Details of the analytical approach are in Appendix C.

Results

The transmission of *B. burgdorferi* from nymphs to mice to larvae is low in systems where either nymphs or larvae are continuously active (Fig. 2). Controlling for total population sizes, when nymphal feeding is evenly spread throughout the year, few nymphs feed at any given time, resulting in limited nymph-to-mouse transmission events. The proportion of infected mice remains constantly low as new infections occur at a similar rate as mouse mortality which replaces older, potentially infected mice with uninfected juveniles. Larval ticks rarely encounter infected mice, thus limiting mouse-to-tick transmission events. By contrast, seasonal nymphal activity concentrates nymph-to-mouse transmission events in time, causing a seasonal peak in mouse infection prevalence that decays with mouse population turnover (Fig. 2). The duration of the nymphal activity period is negatively correlated with the rate at which infected mice accumulate as well as the maximum mouse infection prevalence (*e.g.* small l_n in Fig. 2). That is, nymphal activity periods of greater duration result in a lower maximum mouse infection prevalence that peaks later in the season (Fig. 2). Larval ticks that feed at or around the peak in mouse infection prevalence are more likely to encounter an infected mouse and acquire *B. burgdorferi* before molting to nymphs.

The fitness of *B. burgdorferi*, quantified by the basic reproductive number, is greatest when larval activity is concentrated around the peak in the mouse infection prevalence, thus increasing the probability

that each larva will feed on an infected mouse (Fig. 3A. and Fig. 4A). Larvae that are active substantially after the nymphal activity period ends are likely to feed on an uninfected mouse due to the decay in mouse infection prevalence caused by mouse population turnover (Fig. 3B and Fig. 4B). Similarly, larval activity periods that begin prior to nymphal activity periods result in the majority of larvae feeding on uninfected mice that have not acquired an infection from a feeding nymph.

The effect of the duration of larval emergence depends on whether or not larval emergence coincides with nymphal emergence: for synchronous larval and nymphal emergence, concentrated larval emergence tends to decrease the basic reproductive number (Fig. 5). This happens because with concentrated larval emergence, most larval feeding occurs before nymphs have a chance to increase mouse infection. Conversely, when larvae emerge later than nymphs, concentrated larval emergence tends to increase the basic reproductive number of *B. burgdorferi* (Fig. 6). This happens because with asynchronous emergence, mouse infection prevalence is already high when larvae begin emerging (Fig. 6A), and concentrated emergence results in most larvae feeding when the prevalence of infection is still high. In both cases, the basic reproductive number decreases with very broad larval emergence due to mouse turnover (Fig. 3C, Fig. 4C, Fig. 6B, Fig. 5B).

Discussion

Phenology is a fundamental component of all ecological interactions. Interactions between organisms such as competition, predation, and parasitism are predicated on temporal overlap of interacting species or life-stages.

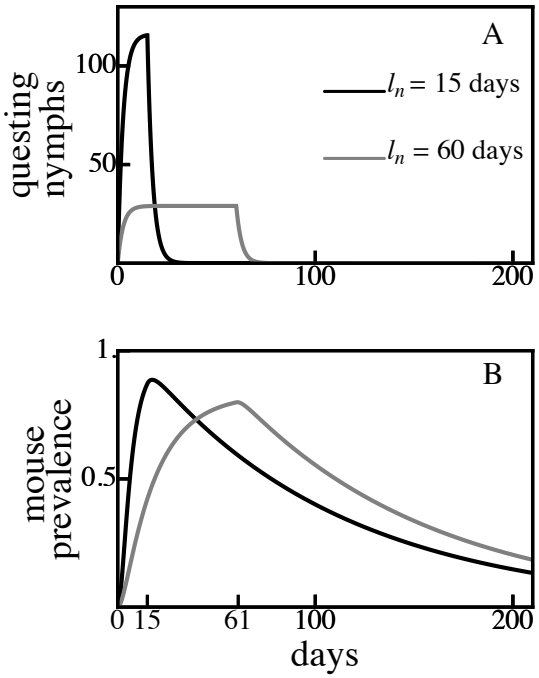

Figure 2: Concentrated nymphal emergence durations ($l_n = 15$ days, (A)) result in a higher and earlier mouse infection prevalence peak compared to longer nymphal emergence durations ($l_n = 60$ days (B)) for the same total tick population sizes. For example, a nymphal activity duration of 15 days ($l_n = 15$ days, (B)) results in peak mouse infection prevalence occurring on day 15 while $l_n = 60$ days results in peak mouse infection prevalence occurring on day 61. In both models, 25% of emerging nymphs are infected, $k = 50, M = k(1 - \mu_m/b) = 45$. All other parameter values are shown in Table 1

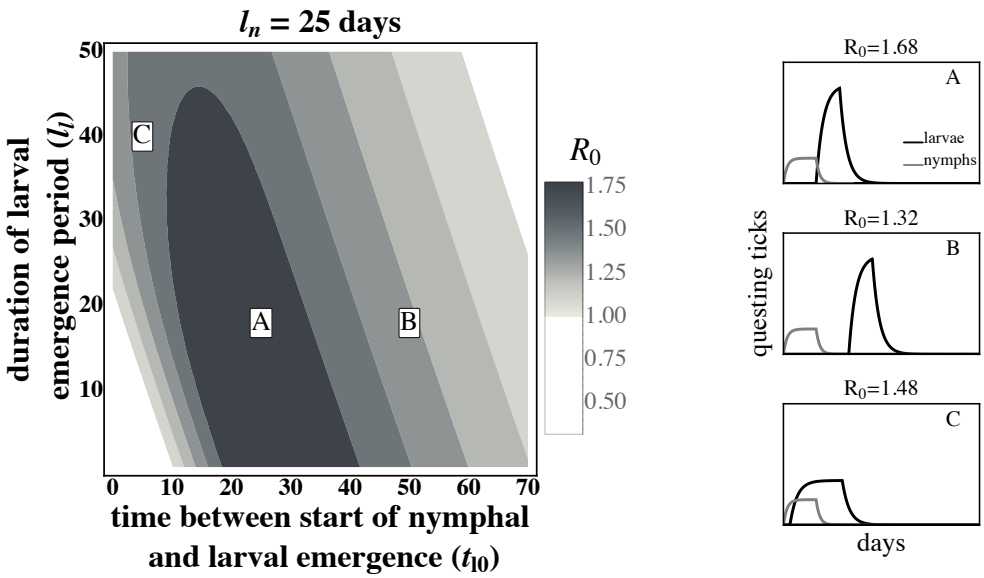

Figure 3: The basic reproductive number, R_0, of *B. burgdorferi* is greatest when larval activity is concentrated around peak mouse infection prevalence. The left-hand side panel depicts the basic reproductive number as a function of the duration of larval emergence (l_l) and time between nymphal and larval emergence (t_{l0}). Panels on the right depict sample within-season dynamics for values of timing parameters indicated by their respective letters on the left hand side panel. (A) Concentrated larval emergence (small l_l) coupled with slight emergence asynchrony ($20 < t_{l0} < 45$) increases the probability that questing larvae feed on mice recently infected by nymphs ($t_{l0} = 25, l_l = 18$). (B) Transmission decreases as larvae emerge later ($t_{l0} > 45$) because the larval cohort feeds after peak mouse infection prevalence ($t_{l0} = 50, l_l = 18$). (C) When larval and nymphal emergence is more synchronous (small t_{l0}), transmission to larvae increases as larval emergence duration increases (large l_l) because more larvae feed after infectious nymphs ($t_{l0} = 5, l_l = 40$). *B. burgdorferi* is not maintained in systems where $R_0 \leq 1$. R_0 is calculated assuming tick emergence is uniformly distributed ($U(l_l)$ where l_l is the larval emergence duration, see Appendix C). $\hat{L} = \hat{L}^*, \hat{N}_i = 1, \hat{N}_u = \hat{N}^* - 1$ (see Appendix A.) $l_n = 25$ days; all other parameter values are shown in Table 1.

Similarly, host or vector phenology impacts parasite fitness by temporally structuring transmission events between interacting hosts or life stages. Host or vector phenological patterns can even determine whether a pathogen is highly-abundant or is unable to persist (Fig. 3). The ubiquity of seasonal activity among hosts and vectors, as well as the geographic variation in seasonal activity patterns, underscores the importance of phenology for the distribution and abundance of many pathogenic microbes including malaria, rabies, tapeworm, and Lyme disease.[23,34–36] Here we derive R_0 for a transmission dynamics model that explicitly considers the impact of phenology on both parasite transmission and vector demography to assess the impact of vector phenology on parasite transmission and fitness using the Lyme disease system as an example. Our results are benchmarked by field data that show a link between the regional differences in tick phenology and differences in *B. burgdorferi* distribution and abundance.[23] Investigation of parameter space in this model revealed the novel insight that large asynchrony between tick-life stages decreases *B. burgdorferi* fitness.

Our model accounts for an important ecological feedback between vector demography and parasite fitness by incorporating the impact of phenology on demography. This is achieved by capturing both within-season infection dynamics and between-season vector demography in our mathematical analysis. Tick population sizes increase with earlier and more concentrated emergence because most ticks have sufficient time to successfully find a host before the season ends. By contrast, late or less concentrated emergence results in fewer ticks feeding before the season ends as the time available for later-emerging ticks to find a

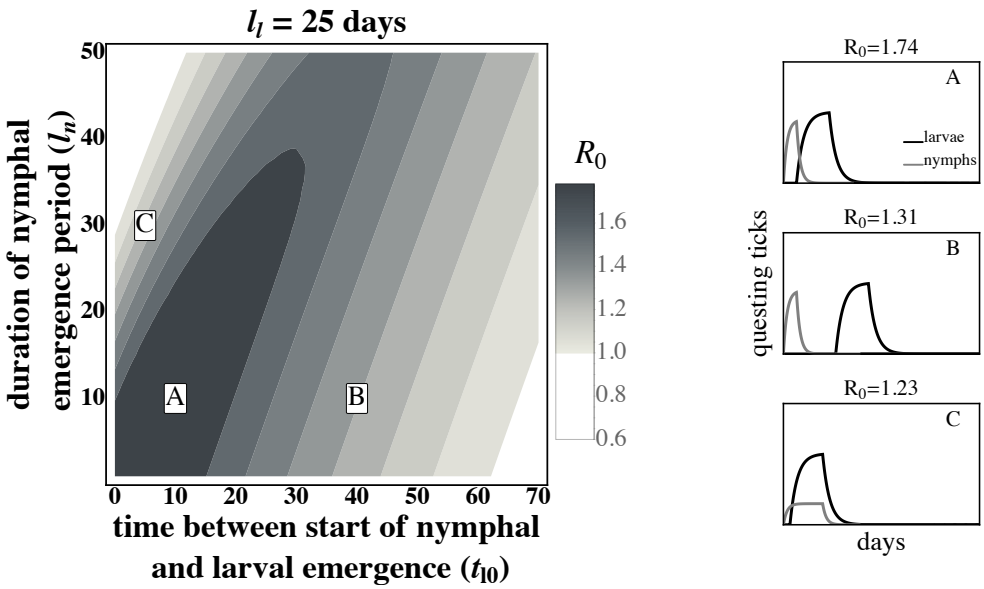

Figure 4: The basic reproductive number, R_0, of *B. burgdorferi* is greatest when larval emergence begins shortly after nymphal emergence such that larvae are active during the peak in mouse infection prevalence. As in Figure 3, the left hand panel depicts R_0, in this case as a function of the time between the start of nymphal and larval emergence (t_{l0}), and the duration of nymphal emergence period (l_n), and the letters indicate the parameters for the within-season dynamics on the right hand panels. (A) Concentrated nymphal emergence (small l_n) coupled with small emergence-time asynchrony between nymphs and larvae ($t_{l0} < 10$) increases the probability questing larvae feed on mice recently infected by nymphs ($t_{l0} = 10, l_n = 10$). (B) Longer emergence-time asynchrony ($t_{l0} > 10$) results in lower mouse-to-larvae transmission rates as many mice infected by nymphs die and are replaced by mice born uninfected such that larvae are likely to feed on uninfected mice ($t_{l0} = 40, l_n = 10$). (C) Synchronous emergence ($t_{l0} = 0$) can also reduce *B. burgdorferi* fitness when nymphal emergence duration is long (large l_n) as many larvae feed before nymphs infect mice ($t_{l0} = 5, l_n = 30$). R_0 is calculated assuming tick emergence is uniformly distributed ($U(l_n)$ where l_n is nymphal emergence length, see Appendix C). $l_l = 25, \hat{L} = \hat{L}^*, \hat{N}_i = 1, \hat{N}_u = \hat{N}^* - 1$ (see Appendix A). All other parameter values are shown in Table 1.

host is effectively shortened. The impact of this feedback is limited at high mouse density but increases rapidly at low mouse density (see Appendix D). Extensions to this framework where vector mortality or contact rates with hosts vary throughout the year are likely to exacerbate the impact of phenology on demography. These results suggest that disregarding between-season demographic dynamics could under-estimate parasite fitness (R_0) when ticks emerge early and over-estimate R_0 when ticks emerge later. The importance of this ecological feedback is reflected in the finding from a next-generation model focusing on within-season (but not between-season) impacts of tick phenology on *B. burgdorferi* fitness which indicated that vector demography is one of the most important model parameters affecting R_0.[25]

Our model captures the impact of phenology on *B. burgdorferi* transmission and fitness in a much simpler modeling framework than previously published studies that address specific hypotheses. In particular, previous work focused on accurately predicting *B. burgdorferi* incidence given phenological scenarios in particular realistic environments and therefore needed several dozens of parameters, all of which require empirical validation.[26] In contrast, our model has 15 parameters and a straightforward structure. This relative simplicity allows our model to serve as a basis for studying phenological impacts in a broader range of environmental scenarios as well as exploring the ramifications of other complicating factors such as

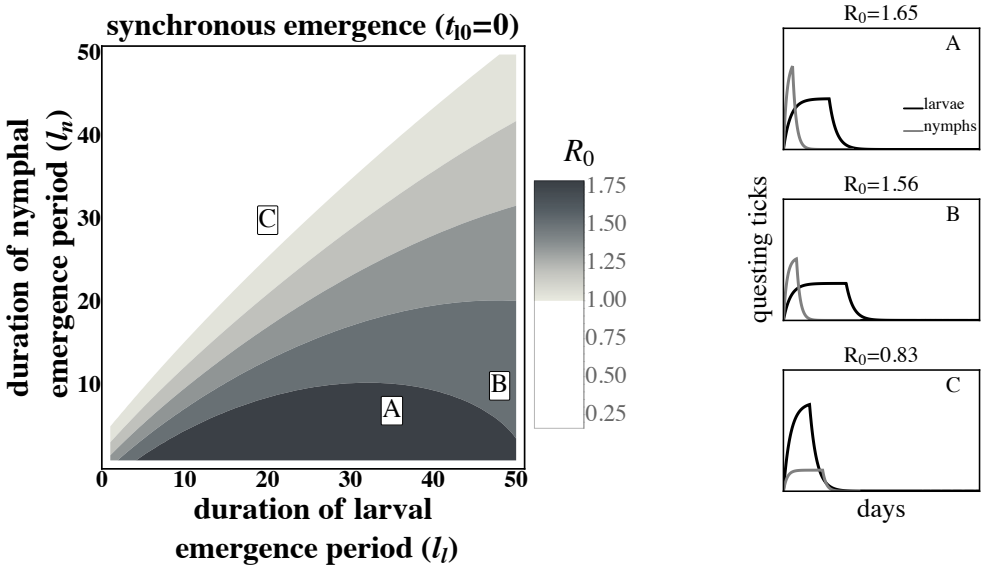

Figure 5: The larval emergence duration that maximizes R_0 for *B. burgdorferi* is conditioned on nymphal emergence duration. R_0 is high if larval emergence duration is slightly longer than nymphal emergence duration ($l_l > l_n$ in A and (B), thus allowing larvae to feed on mice that were previously parasitized by nymphs. However, R_0 decreases when larval emergence duration is much longer than nymphal emergence duration (R_0 of $B < R_0$ of A) as late emerging larvae can feed on uninfected mice born after the nymphal activity period. Transmission from mice to larvae is low when the larval emergence duration is less than the nymphal emergence duration ($l_l < l_n$ in C) because more larvae feed before infectious nymphs. *B. burgdorferi* is not maintained in systems where $R_0 \leq 1$. R_0 is calculated assuming tick emergence is uniformly distributed ($U(l_l)$ where l_l is the larval emergence length. See Appendix C for details). $\hat{L} = \hat{L}^*$, $\hat{N}^* = \hat{N}_u$ - 1 (see Appendix A). $t_{l0} = 0$, (A) $l_l = 35, l_n = 7$ (B) $l_l = 20, l_n = 30$ (B) $l_l = 48, l_n = 10$. $t_{l0} = 0$ days; all other parameter values are shown in Table 1.

the evolutionary dynamics of *B. burgdorferi* virulence.

Parasite fitness is maximized when the activity periods of vector life stages are of short duration (Fig. 2). Continuous nymphal activity temporally distributes the finite number of nymph-to-mouse transmission events such that few mice become infected throughout the season, although rarely. Mouse infection prevalence remains continually low because mice that die, including infected mice, are replaced by uninfected juveniles at rates similar to the rate at which new infections are introduced. Mouse-to-larvae transmission events are similarly rare as most larvae feed on the relatively abundant uninfected mice. By contrast, seasonal nymphal activity concentrates nymph-to-mouse transmission events leading to many new mouse infections over a short period of time. Mouse infection prevalence increases rapidly during the nymphal activity period, as new infections occur at a much greater rate than mouse mortality, and subsequently decline when new infections stop at the end of the nymphal activity period (Fig. 2). Transmission from mice to larvae is very high if larval activity coincides with high mouse infection prevalence (Fig. 3A. and Fig. 4A.) The temporal concentration of infected hosts is likely to have important consequences for the transmission success and fitness of most pathogens.[37,38]

The observed fitness of *B. burgdorferi* in different Lyme disease foci in North America corresponds with model predictions qualitatively. For example, *B. burgdorferi* fitness is relatively low in the Southeastern United States where the activity of both tick developmental stages are comparably continuous throughout the year (Fig. 2).[23] By contrast, *B. burgdorferi* fitness in the Northeastern and mid-Atlantic regions is high

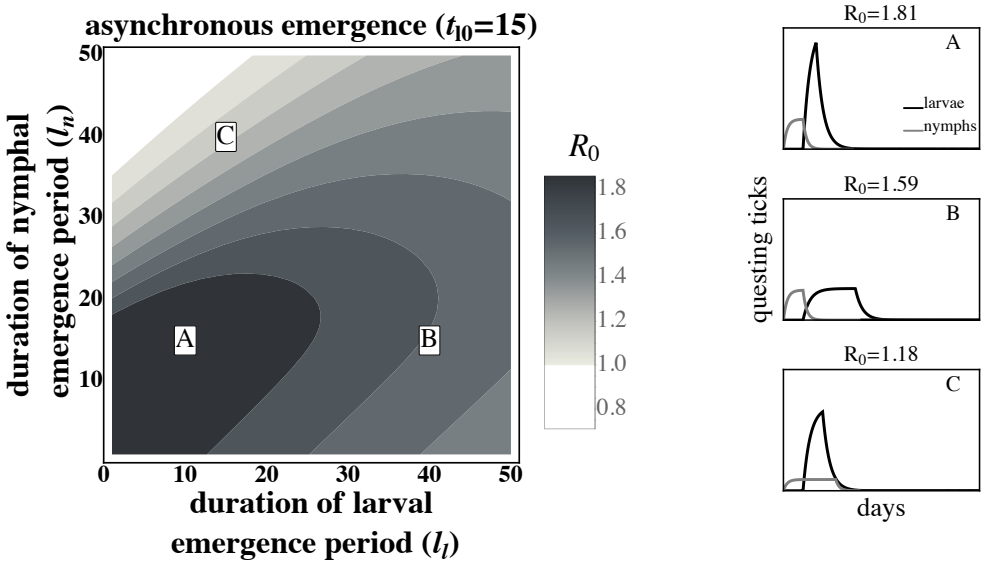

Figure 6: Highly concentrated larval emergence increases R_0 when tick emergence is asynchronous. (A) Concentrated nymphal emergence drives high mouse infection prevalence and results in high transmission to larvae when larval emergence is tightly concentrated ($l_l = 10, l_n = 15$). (B) Transmission from mice to larvae decreases as larval emergence duration increases because larvae are more likely to feed on uninfected mice born after nymphal activity ($l_l = 40, l_n = 15$). (C) Transmission from mice to larvae also decreases if larval emergence duration is highly concentrated and nymphal emergence duration is broad because many larvae feed before nymphs infect mice ($l_l = 15, l_n = 40$). R_0 is calculated assuming tick emergence is $U(l_l)$ where l_l is the larval emergence length (see Appendix C.) $\hat{L} = \hat{L}^*, \hat{N}_i = 1, \hat{N}_u = \hat{N}^* - 1$ (see Appendix A.) $t_{l0} = 15$ days; all other parameter values are shown in Table 1.

due to the pronounced phenological patterns of nymphal and larval ticks (Fig. 2).[23] The concentrated nymphal activity period temporally concentrates tick-to-mouse transmission events, causing a temporary peak in mouse infection prevalence slightly after nymphal feeding (Fig 2). Larval feeding activity concentrated around the mouse infection peak results in *B. burgdorferi* transmission to many larvae (Fig. 3A). In the Midwestern United States, where larvae and nymphs are synchronously active during a limited period, *B. burgdorferi* transmission is lower than in the Northeastern US but much greater than where both stages are more continuously active (Fig. 5). These results show that both the duration of seasonal activity and the relative timing of activity periods impact transmission success and parasite fitness (Figs. 3, 4, 6, 5).

Extended periods between nymphal and larval activity results in limited transmission efficiency (Fig. 3B and Fig. 4B). This novel result for the Lyme disease system is caused by the decay in mouse infection prevalence following nymphal activity due to mouse mortality and the birth of uninfected mice. Thus, larvae feeding long after the nymphal activity period have a greater probability of feeding on uninfected mice than those that feed shortly after the nymphal activity period. While high mouse turnover is the norm in this system,[32] lower mouse turnover would extend the period of high mouse infection prevalence and moderate the declines in parasite fitness caused by extended periods between larval and nymphal emergence.

Parasite fitness is predicted to be greatest when all individuals within each developmental stage feeds simultaneously and larvae feed immediately after nymphs. This result relies on the assumption that there is no limit to the number of ticks that can feed on a mouse at any given time. Realistically, the number of ticks per mouse is limited by grooming and foraging behaviors. Incorporating a maximum number of ticks per

mouse will alter the prediction that simultaneous emergence within life stages maximizes parasite fitness as most ticks will fail to find an available host, resulting in fewer fed ticks each year and thus a lower R_0. Given this more realistic ecological scenario, an intermediately concentrated emergence pattern will result in more infected larvae.

The phenological pattern resulting in the greatest theoretical transmission efficiency occurs when all individuals in each developmental stage feed simultaneously and for larvae to feed immediately after nymphs. This phenological pattern causes all mice to become infected and thus nearly all larvae to feed on an infected host. Realistically, the number of ticks per mouse is limited by grooming and foraging behaviors. Incorporating a maximum capacity of ticks per mouse will alter the prediction that concentrated emergence maximizes transmission efficiency as most larvae will fail to find an available host, resulting in fewer total fed larvae each year and thus a lower R_0. Given this more realistic ecological scenario, an intermediately concentrated emergence pattern will result in more infected larvae.

Our results reveal that slight alterations in host emergence timing can have significant impacts on parasite fitness. This raises the question of whether parasites evolve to manipulate host phenology as observed in the *e.g. Microbotryum violaceum* system where infection causes advances in *Silene alba* flowering time in order to improve transmission opportunities.[39] Manipulation of tick phenology by *B. burgdorferi* has not yet been studied, however it has been suggested that the behavioral changes that have been observed in ticks infected with *B. burgdorferi* increase transmission, but not necessarily tick fitness.[40] Future field experiments could address this question by investigating phenological differences between infected and uninfected nymphs.

As all disease systems exhibit seasonality, phenological drivers may have large impacts on the transmission success, and disease risk from, many parasites. Geographic variation in host or vector phenology may also be an important driver of documented variations in pathogen prevalence and disease risk.[37,38] Public health predictions of disease risk may be improved by accounting for phenological variation. Further, the dramatic shifts in host and vector phenology driven by global climate change[41–44] may result in equally dramatic shifts in pathogen prevalence at regional or global scales.

Author's contributions: HM and DB conceived of the presented idea; HM and EA developed the theoretical framework; HM conducted the mathematical analysis and performed numerical simulations; EA supervised the mathematical analysis and numerical simulations; HM, EA and DB wrote the manuscript; All authors gave final approval for publication and agree to be held accountable for the work performed therein.

This work was supported by the National Institute of Health (T32AI141393 (HM) R01AI142572 (DB), R01AI097137 (DB)); the National Science Foundation (DEB-1354184 (DB)); and the Burroughs Wellcome Fund (1012376 (DB)).

References

[1] Abraham J Miller-Rushing, Toke Thomas Høye, David W Inouye, and Eric Post. The effects of phenological mismatches on demography. Philosophical Transactions of the Royal Society B: Biological Sciences, 365(1555):3177–3186, 2010.

[2] Sharon Bewick, R Stephen Cantrell, Chris Cosner, and William F Fagan. How Resource Phenology Affects Consumer Population Dynamics. The American Naturalist, 187(2):151–166, February 2016.

[3] Sara H Paull and Pieter TJ Johnson. Experimental warming drives a seasonal shift in the timing of host-parasite dynamics with consequences for disease risk. Ecology letters, 17(4):445–453, 2014.

[4] Iain Barber, Boris W Berkhout, and Zalina Ismail. Thermal change and the dynamics of multi-host parasite life cycles in aquatic ecosystems. Integrative and comparative biology, 56(4):561–572, 2016.

[5] Nathan D Burkett-Cadena, Christopher JW McClure, Russell A Ligon, Sean P Graham, Craig Guyer, Geoffrey E Hill, Stephen S Ditchkoff, Micky D Eubanks, Hassan K Hassan, and Thomas R Unnasch. Host reproductive phenology drives seasonal patterns of host use in mosquitoes. PLoS One, 6(3):e17681, 2011.

[6] Elsa E Cleland, Isabelle Chuine, Annette Menzel, Harold A Mooney, and Mark D Schwartz. Shifting plant phenology in response to global change. Trends in Ecology & Evolution, 22(7):357–365, July 2007.

[7] KUDO Gaku, Yoko Nishikawa, Tetsuya Kasagi, and Shoji Kosuge. Does seed production of spring ephemerals decrease when spring comes early? Ecological research, 19(2):255–259, 2004.

[8] David W Inouye. Effects of climate change on phenology, frost damage, and floral abundance of montane wildflowers. Ecology, 89(2):353–362, 2008.

[9] Gaku Kudo and Takashi Y Ida. Early onset of spring increases the phenological mismatch between plants and pollinators. Ecology, 94(10):2311–2320, 2013.

[10] Jane Memmott, Paul G Craze, Nickolas M Waser, and Mary V Price. Global warming and the disruption of plant–pollinator interactions. Ecology letters, 10(8):710–717, 2007.

[11] Stein Joar Hegland, Anders Nielsen, Amparo Lázaro, Anne-Line Bjerknes, and Ørjan Totland. How does climate warming affect plant-pollinator interactions? Ecology letters, 12(2):184–195, 2009.

[12] Abigail E Cahill, Matthew E Aiello-Lammens, M Caitlin Fisher-Reid, Xia Hua, Caitlin J Karanewsky, Hae Yeong Ryu, Gena C Sbeglia, Fabrizio Spagnolo, John B Waldron, Omar Warsi, et al. How does climate change cause extinction? Proceedings of the Royal Society B: Biological Sciences, 280(1750):20121890, 2013.

[13] Derek M Johnson, Ulf Büntgen, David C Frank, Kyrre Kausrud, Kyle J Haynes, Andrew M Liebhold, Jan Esper, and Nils Chr Stenseth. Climatic warming disrupts recurrent alpine insect outbreaks. Proceedings of the National Academy of Sciences, 107(47):20576–20581, 2010.

[14] Jan O Washburn and Howard V Cornell. Parasitoids, patches, and phenology: their possible role in the local extinction of a cynipid gall wasp population. Ecology, 62(6):1597–1607, 1981.

[15] James A Powell and Barbara J Bentz. Connecting phenological predictions with population growth rates for mountain pine beetle, an outbreak insect. Landscape Ecology, 24(5):657–672, 2009.

[16] Jane U Jepsen, Snorre B Hagen, Stein-Rune Karlsen, and Rolf A Ims. Phase-dependent outbreak dynamics of geometrid moth linked to host plant phenology. Proceedings of the Royal Society B: Biological Sciences, 276(1676):4119–4128, 2009.

[17] Margriet van Asch and Marcel E Visser. Phenology of forest caterpillars and their host trees: the importance of synchrony. Annu. Rev. Entomol., 52:37–55, 2007.

[18] Jane U Jepsen, Snorre B Hagen, Rolf A Ims, and Nigel G Yoccoz. Climate change and outbreaks of the geometrids operophtera brumata and epirrita autumnata in subarctic birch forest: evidence of a recent outbreak range expansion. Journal of Animal Ecology, 77(2):257–264, 2008.

[19] A S Clarke. Studies on the life cycle of the pseudophyllidean cestode Schistocephalus solidus. Proceedings of the Zoological Society of London, 124(2):257–302, August 1954.

[20] D C Heins, D M Eidam, and J A Baker. Timing of Infections in the Threespine Stickleback (Gasterosteus aculeatus) by Schistocephalus solidus in Alaska. The Journal of parasitology, 102(2):286–289, April 2016.

[21] S E Randolph. Tick ecology: processes and patterns behind the epidemiological risk posed by ixodid ticks as vectors. Parasitology, 129(7):S37–S65, 1999.

[22] S E Randolph, R M Green, M F Peacey, and D J Rogers. Seasonal synchrony: the key to tick-borne encephalitis foci identified by satellite data. Parasitology, 121 (Pt 1):15–23, July 2000.

[23] Nicholas H Ogden, Genevieve Pang, Howard S Ginsberg, Graham J Hickling, Russell L Burke, Lorenza Beati, and Jean I Tsao. Evidence for geographic variation in life-cycle processes affecting phenology of the lyme disease vector ixodes scapularis (acari: Ixodidae) in the united states. Journal of medical entomology, 55(6):1386–1401, 2018.

[24] R Jory Brinkerhoff, Corrine M Folsom-O'Keefe, Henry M Streby, Stephen J Bent, Kimberly Tsao, and Maria A Diuk-Wasser. Regional variation in immature ixodes scapularis parasitism on north american songbirds: implications for transmission of the lyme pathogen, borrelia burgdorferi. Journal of medical entomology, 48(2):422–428, 2011.

[25] J M Dunn, S Davis, A Stacey, and M A Diuk-Wasser. A simple model for the establishment of tick-borne pathogens of Ixodes scapularis A global sensitivity analysis of R0. Journal of Theoretical Biology, 335(C):213–221, October 2013.

[26] N H Ogden, L R Lindsay, G Beauchamp, D Charron, A Maarouf, C J O'Callaghan, D Waltner-Toews, and I K Barker. Investigation of relationships between temperature and developmental rates of tick Ixodes scapularis (Acari: Ixodidae) in the laboratory and field. Journal of medical entomology, 41(4):622–633, July 2004.

[27] Kathleen LoGiudice, Richard S Ostfeld, Kenneth A Schmidt, and Felicia Keesing. The ecology of infectious disease: effects of host diversity and community composition on Lyme disease risk. Proceedings of the National Academy of Sciences, 100(2):567–571, January 2003.

[28] L A Magnarelli, J F Anderson, and D Fish. Transovarial transmission of Borrelia burgdorferi in Ixodes dammini (Acari:Ixodidae). The Journal of Infectious Diseases, 156(1):234–236, July 1987.

[29] S E Randolph. Tick ecology: processes and patterns behind the epidemiological risk posed by ixodid ticks as vectors. Parasitology, 129(7):S37–S65, 1999.

[30] Stephen Davis and Stephen J Bent. Loop analysis for pathogens: niche partitioning in the transmission graph for pathogens of the north american tick ixodes scapularis. Journal of theoretical biology, 269(1):96–103, 2011.

[31] N H Ogden, M Bigras-Poulin, C J O'Callaghan, I K Barker, L R Lindsay, A Maarouf, K E Smoyer-Tomic, D Waltner-Toews, and D Charron. A dynamic population model to investigate effects of climate on geographic range and seasonality of the tick Ixodes scapularis. International Journal for Parasitology, 35(4):375–389, April 2005.

[32] Malcolm D Schug, Stephen H Vessey, and Andrew I Korytko. Longevity and Survival in a Population of White-Footed Mice (Peromyscus leucopus) . American Society of Mammologists, 72(2):360–366, May 1991.

[33] H McCallum. How should pathogen transmission be modelled? Trends in Ecology & Evolution, 16(6):295–300, June 2001.

[34] Moshe B Hoshen and Andrew P Morse. A weather-driven model of malaria transmission. Malaria journal, 3(1):32, 2004.

[35] Catherine Gremillion-Smith and Alan Woolf. Epizootiology of skunk rabies in north america. Journal of wildlife diseases, 24(4):620–626, 1988.

[36] Roy M Anderson. Population dynamics of the cestode caryophyllaeus laticeps (pallas, 1781) in the bream (abramis brama l.). The Journal of Animal Ecology, pages 305–321, 1974.

[37] Sonia Altizer, Andrew Dobson, Parviez Hosseini, Peter Hudson, Mercedes Pascual, and Pejman Rohani. Seasonality and the dynamics of infectious diseases. Ecology Letters, 9(4):467–484, March 2006.

[38] Micaela Elvira Martinez. The calendar of epidemics: Seasonal cycles of infectious diseases. PLOS Pathogens, 14(11):e1007327–15, November 2018.

[39] Helen Miller Alexander. An experimental field study of anther-smut disease of Silene alba caused by Ustilago violacea: genotypic variation and disease incidence . Evolution, 43(4):835–847, July 1989.

[40] H Lefcort and L A Durden. The effect of infection with Lyme disease spirochetes (Borrelia burgdorferi) on the phototaxis, activity, and questing height of the tick vector Ixodes scapularis. Parasitology, 113:97–103, March 1996.

[41] J Penuelas. Phenology: Responses to a Warming World. Science, 294(5543):793–795, October 2001.

[42] Leo Meyer, Sander Brinkman, Line van Kesteren, Noëmie Leprince-Ringuet, and Fijke van Boxmeer. IPCC, 2014: Climate Change 2014: Synthesis Report. Contribution of Working Groups I, II and III to the Fifth Assessment Report of theIntergovernmental Panel on Climate Change. Technical report, Geneva, Switzerland, 2014.

[43] E Post, M C Forchhammer, N C Stenseth, and T V Callaghan. The timing of life-history events in a changing climate. Proceedings of the Royal Society B: Biological Sciences, 268(1462):15–23, January 2001.

[44] Jacob Johansson, Jan-Åke Nilsson, and Niclas Jonzén. Phenological change and ecological interactions: an introduction. Oikos, 124(1):1–3, December 2014.

Appendix A

In Appendix A we derive between-season equilibrial solutions for tick demography (A.1a - A.1d), ignoring infection status. The following differential equations describe within-season tick population dynamics, valid from (0, τ) where τ is the length of the tick feeding season. For simplicity, we assume that the mouse population is constant so that $M = k(1 - \frac{\mu_m}{b})$ where b is the mouse birth rate, k is the carrying capacity and μ_m is the mouse death rate. All other parameters are the same as described in the main text.

$$\frac{dL_q}{dt} = \hat{L}(T)g_l(t, \theta_l) - L_q(\gamma_l M + \mu_l), \tag{A.1a}$$

$$\frac{dL_f}{dt} = \gamma_l L_q M, \tag{A.1b}$$

$$\frac{dN_q}{dt} = \hat{N}(T)g_n(t, \theta_n) - N_q(\gamma_n M + \mu_n), \tag{A.1c}$$

$$\frac{dN_f}{dt} = \gamma_n N_q M. \tag{A.1d}$$

(A.1a-d) is solved analytically by describing tick emergence using a uniform distribution

$$g_\bullet(t, l_\bullet) = \begin{cases} 0 & t < t_{\bullet 0} \\ \frac{1}{l_\bullet} & t_{\bullet 0} \leq t \leq t_{\bullet f} \\ 0 & t_{\bullet f} < \tau \end{cases}$$

Within-season dynamics are coupled to recurrence equations that describe nymphal and larval survival between years. The total fed larval population at the end of the year, $L_f(\tau)$ gives rise to the population of nymphs $\hat{N}$ that will emerge the following year, described by the map

$$\hat{N}(T+1) = \sigma_l L_f(\tau)$$

Where σ_l accounts for the survival between fed larvae and questing nymphs and the number of fed larvae at time τ is given by

$$L_f(\tau) = \frac{\gamma_l \hat{L}(T)M}{l_l(\gamma_l M + \mu_l)}\left(\int_{t_{l0}}^{t_{lf}} 1 - e^{-(\gamma_l M + \mu_l)x}dx + (1 - e^{-(\gamma_l M + \mu_l)l_l})\int_0^{\tau - t_{lf}} e^{-(\gamma_l M + \mu_l)x}dx\right)$$

Similarly, the total fed nymphal population at the end of the year, $N_f(\tau)$, gives rise to the population of larvae $\hat{L}$ that will emerge the following year, described by the map

$$\hat{L}(T+1) = \frac{\sigma_n N_f(\tau)}{1 + \alpha N_f(\tau))}$$

This expression accounts for the expected number of questing larvae produced per nymph that feeds to repletion after accounting for survival through adulthood, density dependent adult fecundity and survival

from egg to questing larva. The number of fed nymphs at time τ is given by

$$N_f(\tau) = \frac{\gamma_n \hat{N}(T) M}{l_n(\gamma_n M + \mu_n)} \left(\int_0^{t_{nf}} 1 - e^{-(\gamma_n M + \mu_n)x} dx + (1 - e^{-(\gamma_n M + \mu_n) l_n}) \int_0^{\tau - t_{nf}} e^{-(\gamma_n M + \mu_n)x} dx \right)$$

If we define

$$\phi_l = \frac{\gamma_l M}{l_l(\gamma_l M + \mu_l)} \left(\int_{t_{l0}}^{t_{lf}} 1 - e^{-(\gamma_l M + \mu_l)x} dx + (1 - e^{-(\gamma_l M + \mu_l) l_l}) \int_0^{\tau - t_{lf}} e^{-(\gamma_l M + \mu_l)x} dx \right),$$

$$\phi_n = \frac{\sigma_n \gamma_n M}{l_n(\gamma_n M + \mu_n)} \left(\int_0^{t_{nf}} 1 - e^{-(\gamma_n M + \mu_n)x} dx + (1 - e^{-(\gamma_n M + \mu_n) l_n}) \int_0^{\tau - t_{nf}} e^{-(\gamma_n M + \mu_n)x} dx \right)$$

The maps for $\hat{L}(T+1)$ and $\hat{N}(T+1)$ can be written as

$$\hat{L}(T+1) = \frac{\sigma_n \phi_n \hat{N}(T)}{1 + \alpha \phi_n \hat{N}(T)},$$
$$\hat{N}(T+1) = \sigma_l \phi_l \hat{L}(T)$$

The equilibrium population size $\hat{L}^*$ is then

$$\hat{L}(T+2) = \frac{\sigma_n \phi_n \hat{N}(T+1)}{1 + \alpha \phi_n \hat{N}(T+1)},$$
$$\hat{L}(T+2) = \frac{\sigma_n \sigma_l \phi_n \phi_l \hat{L}(T)}{1 + \alpha \sigma_l \phi_n \phi_l \hat{L}(T)})$$
$$\hat{L}^* = \frac{\sigma_n \sigma_l \phi_n \phi_l \hat{L}^*}{1 + \alpha \sigma_l \phi_n \phi_l \hat{L}^*})$$
$$\hat{L}^* = \frac{\sigma_n \sigma_l \phi_n \phi_l - 1}{\alpha \sigma_l \phi_n \phi_l}$$

Similarly for $\hat{N}^*$

$$\hat{N}(T+2) = \sigma_l \phi_l \hat{L}(T+1)$$
$$\hat{N}(T+2) = \frac{\sigma_n \sigma_l \phi_n \phi_l \hat{N}(T)}{1 + \alpha \phi_n \hat{N}(T)}$$
$$\hat{N}^* = \frac{\sigma_n \sigma_l \phi_n \phi_l \hat{N}^*}{1 + \alpha \phi_n \hat{N}^*}$$
$$\hat{N}^* = \frac{\sigma_n \sigma_l \phi_n \phi_l - 1}{\alpha \phi_n}$$

The stability of these equilibrium points is found by considering the biennial maps of the tick life cycle

$$\frac{d\hat{L}(T+2)}{d\hat{L}(T)}\Big|_{\hat{L}(T)=L^*} = -\frac{\sigma_n\sigma_l\phi_n\phi_l}{(1+\alpha\sigma_l\phi_n\phi_l\hat{L}^*)^2}$$
$$\frac{d\hat{L}(T+2)}{d\hat{L}(T)}\Big|_{\hat{L}(T)=L^*} = \frac{1}{\sigma_n\sigma_l\phi_n\phi_l}$$

This system is stable for $\sigma_n\sigma_l\phi_n\phi_l > 1$. σ_n, ϕ_n, and ϕ_l are always less than 1. Therefore, the stability of the tick demographic equilibrium depends on maintaining $\sigma_l\phi_n\phi_l < \frac{1}{\sigma_n}$.
Figures in the main text assume both tick life-stages are at equilibrium by using L^* and N^* for the sizes of emerging tick cohorts at the beginning of the season. ($\hat{L}(T) = L^*, \hat{N}_i(T) + \hat{N}_u(T) = N^*$).

Appendix B

In Appendix B we derive analytical solutions for Equations (1a-1g) from the main text. Equations (1a-1g) reduce to the following set of equations if we assume that the host population is at equilibrium, ($M = k(1 - \frac{\mu_m}{b})$):

$$\frac{dL_q}{dt} = \hat{L}(T)g_l(t,\theta_l) - L_q(\gamma_l M + \mu_l), \tag{B.1a}$$
$$\frac{dL_{if}}{dt} = \beta_{ml}\gamma_l L_q M_i - \mu_f L_q, \tag{B.1b}$$
$$\frac{dL_{uf}}{dt} = \gamma_l L_q(M - \beta_{ml}M_i) - \mu_f L_q, \tag{B.1c}$$
$$\frac{dN_{iq}}{dt} = \hat{N}_i(T)g_n(t,\theta_n) - N_{iq}(\gamma_n M + \mu_n), \tag{B.1d}$$
$$\frac{dN_{uq}}{dt} = \hat{N}_u(T)g_n(t,\theta_n) - N_{uq}(\gamma_n M + \mu_n), \tag{B.1e}$$
$$\frac{dN_f}{dt} = \gamma_n(N_{iq} + N_{uq}) - \mu_f N_f, \tag{B.1f}$$
$$\frac{dM_i}{dt} = \beta_{nm}\gamma_n N_{iq}(M - M_i) - \mu_m M_i. \tag{B.1g}$$

The system (B.1a-g) is solved analytically by describing tick emergence using a uniform distribution

$$g_\bullet(t, l_\bullet) = \begin{cases} 0 & t < t_{\bullet 0} \\ \frac{1}{l_\bullet} & t_{\bullet 0} \le t \le t_{\bullet f} \\ 0 & t_{\bullet f} < \tau \end{cases}$$

where $t_{\bullet 0}$ denotes the start of emergence, $l_\bullet$ denotes the length of emergence and $t_{\bullet f}$ denotes the end of emergence ($t_{\bullet 0} + l_\bullet = t_{\bullet f}$). The season begins with the emergence of the nymphs ($t_{n0} = 0$). Larval emergence, t_{l0} can begin concurrently with nymphal emergence ($t_{l0} = 0$) or have a start time that is offset

relative to nymphs ($t_{l0} > 0$). The within-season dynamics have the following time-dependent solutions:

$$L_q(t) = \begin{cases} 0 & t < t_{l0} \\ \frac{\hat{L}(T)}{l_l(\gamma_l M+\mu_l)}(1-e^{-(\gamma_l M+\mu_l)t}) & t_{l0} \le t \le t_{lf} \\ L_q(t_{lf})e^{-(\gamma_l M+\mu_l)t} & t_{lf} < \tau \end{cases} \tag{B.2a}$$

$$L_{if}(t) = \begin{cases} 0 & t < t_{l0} \\ \frac{\gamma_l \beta_{ml}\hat{L}(T)}{l_l(\gamma_l M+\mu_l)}(\int_{t_{l0}}^{t_{lf}} 1-e^{-(\gamma_l M+\mu_l)x}\int_0^x M_i(s+t_{l0})dsdx & t_{l0} \le t \le t_{lf} \\ \gamma_l \beta_{ml} L_{if}(t_{lf})\int_0^{T-t_{lf}} e^{-(\gamma_l M+\mu_l)x}\int_0^x M_i(s+t_{lf})dsdx & t_{lf} < \tau \end{cases} \tag{B.2b}$$

$$L_{uf}(t) = \begin{cases} 0 & t < t_{l0} \\ \frac{\gamma_l \hat{L(T)}}{l_l(\gamma_l M+\mu_l)}(\int_{t_{l0}}^{t_{lf}} 1-e^{-(\gamma_l M+\mu_l)x}\int_0^x (M-\beta_{ml}M_i(s+t_{l0}))dsdx & t_{l0} \le t \le t_{lf} \\ \gamma_l L_{uf}(t_{lf})\int_0^{T-t_{lf}} e^{-(\gamma_l M+\mu_l)x}\int_0^x (M-\beta_{ml}M_i(s+t_{lf}))dsdx & t_{lf} < \tau \end{cases} \tag{B.2c}$$

$$N_{iq}(t) = \begin{cases} \frac{\hat{N}_i(T)}{l_n(\gamma_n M+\mu_n)}(1-e^{-(\gamma_n M+\mu_n)t}) & 0 \le t \le t_{nf} \\ N_{iq}(t_{nf})e^{-(\gamma_n M+\mu_n)t} & t_{nf} < \tau \end{cases} \tag{B.2d}$$

$$N_{uq}(t) = \begin{cases} \frac{\hat{N}_u(T)}{l_n(\gamma_n M+\mu_n)}(1-e^{-(\gamma_n M+\mu_n)t}) & 0 \le t \le t_{nf} \\ N_{uq}(t_{nf})e^{-(\gamma_n M+\mu_n)t} & t_{nf} < \tau \end{cases} \tag{B.2e}$$

$$N_f(t) = \begin{cases} \frac{\gamma_n M(\hat{N}_i(T)+\hat{N}_u(T))}{l_n(\gamma_n M+\mu_n)}\int_0^{t_{nf}}(1-e^{-(\gamma_n M+\mu_n)s})ds & 0 \le t \le t_{nf} \\ N_f(t_{nf})\int_0^{T-t_{nf}} e^{-(\gamma_n M+\mu_n)s}ds & t_{nf} < t < \tau \end{cases} \tag{B.2f}$$

$$M_i(t) = \begin{cases} \frac{\gamma_n \beta_{nm}\hat{N}_i(T)M}{l_n(\gamma_n M+\mu_n)}M_{i1}(t,\hat{N}_i(T)) & 0 \le t \le t_{nf} \\ \frac{\gamma_n \beta_{nm}\hat{N}_i(T)M}{l_n(\gamma_n M+\mu_n)}M_{i2}(t,\hat{N}_i(T)) & t_{nf} < t < \tau \end{cases} \tag{B.2g}$$

(B.2g) depends on the activity of questing nymphs and is split by whether nymphs are emerging (new nymphs entering system), $M_{i1}(t)$ for $0 \le t \le t_{nf}$ or have finished emerging (no more new nymphs entering system), $M_{i2}(t)$ for $t_{nf} < t < \tau$.

$$\begin{aligned} M_{i1}(t,\hat{N}_i(T)) =& e^{-\mu_n t - \frac{e^{-(\gamma_n M+\mu_n)M}\gamma_n \beta_{nm}\hat{N}_i(T)(1+e^{-(\gamma_n M+\mu_n)t}(\gamma_n M+\mu_n)t)}{l_n(\gamma_n M+\mu_n)^2}} \\ & \int_0^t -e^{\frac{-e^{-(\gamma_n M+\mu_n)}\gamma_n \beta_{nm}\hat{N}_i(T)+(\gamma_n M+\mu_n)(\gamma_n \beta_{nm}\hat{N}_i(T)+l_n \mu_m(\gamma_n M+\mu_n))s}{l_n(\gamma_n M+\mu_n)^2}(-1+e^{-(\gamma_n M+\mu_n)s})}ds \\ M_{i2}(t,\hat{N}_i(T)) =& e^{-\mu_n t + \frac{e^{-(\gamma_n M+\mu_n)t}\gamma_n \beta_{nm}N_{iq}(t_{nf})}{\gamma_n M+\mu_n}}(e^{-\frac{\gamma_n \beta_{nm}N_{iq}(t_{nf})}{\gamma_n M+\mu_n}}M_{i1}(t_{nf},\hat{N}_i(T)) + \\ & \gamma_n \beta_{nm}N_{iq}(t_{nf})M\int_0^t e^{\frac{-e^{-(\gamma_n M+\mu_n)s}\gamma_n \beta_{nm}N_{iq}(t_{nf})}{\gamma_n M+\mu_n}-(\gamma_n M-\mu_m+\mu_n)s}) \end{aligned}$$

The total number of fed infected larvae by the end of the season, $L_{if}(\tau)$, fed uninfected larvae by the end of

the season, $L_{uf}(\tau)$ and total fed larvae by the end of the season $L_f(\tau)$ are given by

$$\begin{aligned}
L_{if}(\tau) =& \frac{\gamma_l \beta_{ml} \hat{L}(T)}{l_l(\gamma_l M + \mu_l)} \Big(\int_{t_{l0}}^{t_{lf}} 1 - e^{-(\gamma_l M + \mu_l)x} \int_0^x M_i(s + t_{l0}) ds dx + \\
& (1 - e^{-(\gamma_l M + \mu_l) l_l}) \int_0^{\tau - t_{lf}} e^{-(\gamma_l M + \mu_l)x} \int_0^x M_i(s + t_{lf}) ds dx \Big) \\
L_{uf}(\tau) =& \frac{\gamma_l \hat{L}(T)}{l_l(\gamma_l M + \mu_l)} \Big(\int_{t_{l0}}^{t_{lf}} 1 - e^{-(\gamma_l M + \mu_l)x} \int_0^x 1 - \beta_{ml} M_i(s + t_{l0}) ds dx + \\
& (1 - e^{-(\gamma_l M + \mu_l) l_l}) \int_0^{\tau - t_{lf}} e^{-(\gamma_l M + \mu_l)x} \int_0^x 1 - \beta_{ml} M_i(s + t_{lf}) ds dx \Big) \\
L_f(\tau) =& \frac{\gamma_l \hat{L}(T) M}{l_l(\gamma_l M + \mu_l)} \Big(\int_{t_{l0}}^{t_{lf}} 1 - e^{-(\gamma_l M + \mu_l)x} dx + (1 - e^{-(\gamma_l M + \mu_l) l_l}) \int_0^{\tau - t_{lf}} e^{-(\gamma_l M + \mu_l)x} dx \Big)
\end{aligned}$$

Note that both $L_{if}(\tau)$ and $L_{uf}(\tau)$ are dependent on $\hat{N}_i$ through the transmission dynamics of $M_i(t)$. The total number of fed nymphs by the end of the season is given by

$$N_f(\tau) = \frac{\sigma_n \gamma_n (\hat{N}_i(T) + \hat{N}_u(T)) M}{l_n(\gamma_n M + \mu_n)} \Big(\int_0^{t_{nf}} 1 - e^{-(\gamma_n M + \mu_n)x} dx + (1 - e^{-(\gamma_n M + \mu_n) l_n}) \int_0^{\tau - t_{nf}} e^{-(\gamma_n M + \mu_n)x} dx \Big)$$

We can also write $L_{if}(\tau)$, $L_{uf}(\tau)$ and $N_f(\tau)$ in terms of the total number of emerging ticks for a given season, $\hat{L}(T)$, $\hat{N}_i(T)$, and $\hat{N}_u(T)$.

$$\begin{aligned}
L_{if}(\tau) =& \phi_{li}(\hat{N}_i(T)) \hat{L}(T), \\
L_{uf}(\tau) =& \phi_{lu}(\hat{N}_u(T)) \hat{L}(T), \\
N_f(\tau) =& \phi_n \hat{N}(T).
\end{aligned}$$

Where ϕ_n denotes the fraction of emerging nymphs that feed over a season as calculated from within-season dynamics and $\phi_{li}(\hat{N}_i(T))$ and $\phi_{lu}(\hat{N}_i(T))$ are functions of $\hat{N}_i(T)$ that denote the fraction of emerging larvae that feed and become infected or remain uninfected respectively, as calculated from within-season dynamics.

$$\begin{aligned}
\phi_{li}(\hat{N}_i(T)) =& \frac{\gamma_l \beta_{ml}}{l_l(\gamma_l M + \mu_l)} \Big(\int_{t_{l0}}^{t_{lf}} 1 - e^{-(\gamma_l M + \mu_l)x} \int_0^x M_i(s + t_{l0}, \hat{N}_i(T)) ds dx + \\
& (1 - e^{-(\gamma_l M + \mu_l) l_l}) \int_0^{\tau - t_{lf}} e^{-(\gamma_l M + \mu_l)x} \int_0^x M_i(s + t_{lf}, \hat{N}_i(T)) ds dx \Big), \\
\phi_{lu}(\hat{N}_i(T)) =& \frac{\gamma_l}{l_l(\gamma_l M + \mu_l)} \Big(\int_{t_{l0}}^{t_{lf}} 1 - e^{-(\gamma_l M + \mu_l)x} \int_0^x 1 - \beta_{ml} M_i(s + t_{l0}, \hat{N}_i(T)) ds dx + \\
& (1 - e^{-(\gamma_l M + \mu_l) l_l}) \int_0^{\tau - t_{lf}} e^{-(\gamma_l M + \mu_l)x} \int_0^x 1 - \beta_{ml} M_i(s + t_{lf}, \hat{N}_i(T)) ds dx \Big), \\
\phi_n =& \frac{\sigma_n \gamma_n M}{l_n(\gamma_n M + \mu_n)} \Big(\int_0^{t_{nf}} 1 - e^{-(\gamma_n M + \mu_n)x} dx + (1 - e^{-(\gamma_n M + \mu_n) l_n}) \int_0^{\tau - t_{nf}} e^{-(\gamma_n M + \mu_n)x} dx \Big).
\end{aligned}$$

Discrete annual maps of each population can then be written as

$$\hat{L}(T+1) = \frac{\sigma_n \phi_n \hat{N}(T)}{1 + \alpha \phi_n \hat{N}(T))},$$
$$\hat{N}_i(T+1) = \sigma_l \phi_{li}(\hat{N}_i(T))\hat{L}(T),$$
$$\hat{N}_u(T+1) = \sigma_l \phi_{lu}(\hat{N}_i(T))\hat{L}(T),$$

To check the stability of tick populations, consider the biennial maps

$$\hat{L}(T+2) = \frac{\sigma_n \sigma_l \phi_n \phi_l \hat{L}(T)}{1 + \alpha \sigma_l \phi_n \phi_l \hat{L}(T)},$$
$$\hat{N}_i(T+2) = \frac{\sigma_l \sigma_n \phi_n \phi_{li}(\hat{N}_i(T))\hat{N}(T)}{1 + \alpha \phi_n \hat{N}(T)},$$
$$\hat{N}_u(T+2) = \frac{\sigma_l \sigma_n \phi_n \phi_{lu}(\hat{N}_i(T))\hat{N}(T)}{1 + \alpha \phi_n \hat{N}(T)}$$

Infection status does not impact demographic rates. Therefore the larval equilibrium size $\hat{L}*$ and total nymphal equilibrium size $\hat{N}^*$ in the infection subsystem are identical to the result found above in Appendix A that ignores infection. $\hat{N}_i^*$ and $\hat{N}_u^*$ are both stable for the same conditions given in Appendix A because they are upper bounded by $\hat{N}^*$ ($\hat{N}_i^* + \hat{N}_u^* = \hat{N}^*$). Assuming the stability conditions in Appendix A are met, the nontrivial solutions for $\hat{N}_i^*$ and $\hat{N}_u^*$ are unique because $\phi_{li}, \phi_{lu} < 1$ and the transmission terms are $0 < \beta_{nm}, \beta_{ml} < 1$.

$$\hat{N}_i^* = \frac{\sigma_l \sigma_n \phi_n \phi_{li}(\hat{N}_i^*)\hat{N}^*}{1 + \alpha \phi_n \hat{N}^*},$$
$$\hat{N}_u* = \frac{\sigma_l \sigma_n \phi_n \phi_{lu}(\hat{N}_i^*)\hat{N}^*}{1 + \alpha \phi_n \hat{N}^*}$$

Appendix C

In Appendix C we derive R_0 to study how phenology impacts thresholds for parasite persistence. R_0 is computed as the number of infected nymphs that emerge in year $T+1$ produced by a single infected nymph that emerged in year T in an otherwise uninfected population. Specifically, we consider the stabiliy of the disease-free equilibrium when a rare infected nymph is introduced into the tick population, solved by setting $\hat{L}^* = \hat{L}(T)$, $\hat{N}^* = \hat{N}_u(T) - 1$, and $\hat{N}_i(T) = 1$ in equations (5) and (7).

Three distinct cases of phenological patterns are relevant to this system: (1) Emergence of both tick stages overlap and larvae finish emerging before nymphs finish emerging (2) Emergence of both tick stages overlap and nymphs finish emerging before larvae finish emerging (3) Nymph emergence ends before larvae emergence begins. Each case needs to be analyzed separately to account for the time dependent differences in the dynamics.

Using Case 1 as an example to sketch our derivation:

$$\hat{N}_i(T+1) = \sigma_l \phi_{li}(\hat{N}_i)\hat{L}^*$$
$$\hat{N}_i(T+1) = \frac{\sigma_l \gamma_l \beta_{ml}\hat{L}^*}{l_l(\gamma_l M + \mu_l)} \frac{\gamma_n \beta_{nm}\hat{N}_i(T)M}{l_n(\gamma_n M + \mu_n)} (\int_0^{t_{lf}-t_{l0}} 1 - e^{-(\gamma_l M+\mu_l)x} \int_0^x M_{i1}(s+t_{l0}, \hat{N}_i(T))dsdx$$
$$+ \int_0^{t_{nf}-t_{lf}} e^{-(\gamma_l M+\mu_l)x} \int_0^x M_{i1}(s+t_{lf}, \hat{N}_i(T))dsdx + \int_0^{\tau-t_{nf}} e^{-(\gamma_l M+\mu_l)(x+t_{nf}-t_{lf})} \int_0^x M_{i2}(s, \hat{N}_i(T))dsdx)$$
$$R_0 = \frac{\hat{N}_i(T+1)}{\hat{N}_i(T)} = \frac{\sigma_l \gamma_l \beta_{ml}\hat{L}^*}{l_l(\gamma_l M + \mu_l)} \frac{\gamma_n \beta_{nm}M}{l_n(\gamma_n M + \mu_n)} (\int_0^{t_{lf}-t_{l0}} 1 - e^{-(\gamma_l M+\mu_l)x} \int_0^x M_{i1}(s+t_{l0}, \hat{N}_i(T))dsdx)$$
$$+ (\int_0^{t_{nf}-t_{lf}} e^{-(\gamma_l M+\mu_l)x} \int_0^x M_{i1}(s+t_{lf}, \hat{N}_i(T))dsdx + \int_0^{\tau-t_{nf}} e^{-(\gamma_l M+\mu_l)(x+t_{nf}-t_{lf})} \int_0^x M_{i2}(s, \hat{N}_i(T))dsdx)$$

for $\hat{N}_i(T) = 1$, parasites persist in phenological scenarios where $\hat{N}_i(T+1) \geq 1$. Parasite fitness is maximized when peak larval activity coincides with peak host prevalence.
When $R_0 > 1$, the number of infected nymphs, $\hat{N}_i$ reaches a stable T-periodic equilibrium

$$\hat{N}_i^* = \hat{N}^* - \hat{N}_u^*$$

$\hat{N}_i^*$ for a given phenological scenario can be found by solving for the value of $\hat{N}_i$ that satisfies $R_0 = 1$. Again, using Case 1 as an example:

$$1 = \sigma_l(L_f(\tau)) \frac{\gamma_l \beta_{ml}\hat{L}^*}{l_l(\gamma_l M + \mu_l)} \frac{\gamma_n \beta_{nm}M}{l_n(\gamma_n M + \mu_n)} (\int_0^{t_{lf}-t_{l0}} 1 - e^{-(\gamma_l M+\mu_l)x} \int_0^x M_{i1}(s+t_{l0}, \hat{N}_i^*)dsdx)$$
$$+ L_q(t_{lf}) \frac{\gamma_n \beta_{nm}M}{l_n(\gamma_n M + \mu_n)} (\int_0^{t_{nf}-t_{lf}} e^{-(\gamma_l M+\mu_l)x} \int_0^x M_{i1}(s+t_{lf}, \hat{N}_i^*)dsdx$$
$$+ \int_0^{\tau-t_{nf}} e^{-(\gamma_l M+\mu_l)(x+t_{nf}-t_{lf})} \int_0^x M_{i2}(s, \hat{N}_i^*)dsdx)$$

If the total tick population is stable (see Appendix A), $\hat{N}_i^*$ is upper bounded by $\hat{N}^*$ and is therefore stable as well.

Appendix D

In Appendix D we demonstrate that tick phenological patterns can alter tick equilibrium population sizes and impact R_0. Not accounting for the impact of phenology on between-season tick population demography by assuming constant tick populations each year leads to over or under estimates of tick demography (Figure A-1) and parasite fitness (Figures A-2,A-3). Our model in contrast accounts for the feedback between vector demography and parasite fitness by considering both within-season transmission and vector population dynamics (see Appendix B and C) and between-season vector demography (see Appendix A and B). Mouse density impacts R_0 (Figure A-4); the error in R_0 estimate when not accounting for population dynamics is especially high when mouse density is low.

R_0 is a function of the equilibrium larval population size, $\hat{L}^*$, which is in turn determined by tick

phenology (see equation (A.3) in Appendix A).

$$R_0 = \frac{\hat{N}_i(T+1)}{\hat{N}_i(T)} = \sigma_l \phi_{li}(\hat{N}_i)\hat{L}^*$$

The ecological feedback between tick phenology, tick demography and R_0 is ignored if a constant $\hat{L}$ is

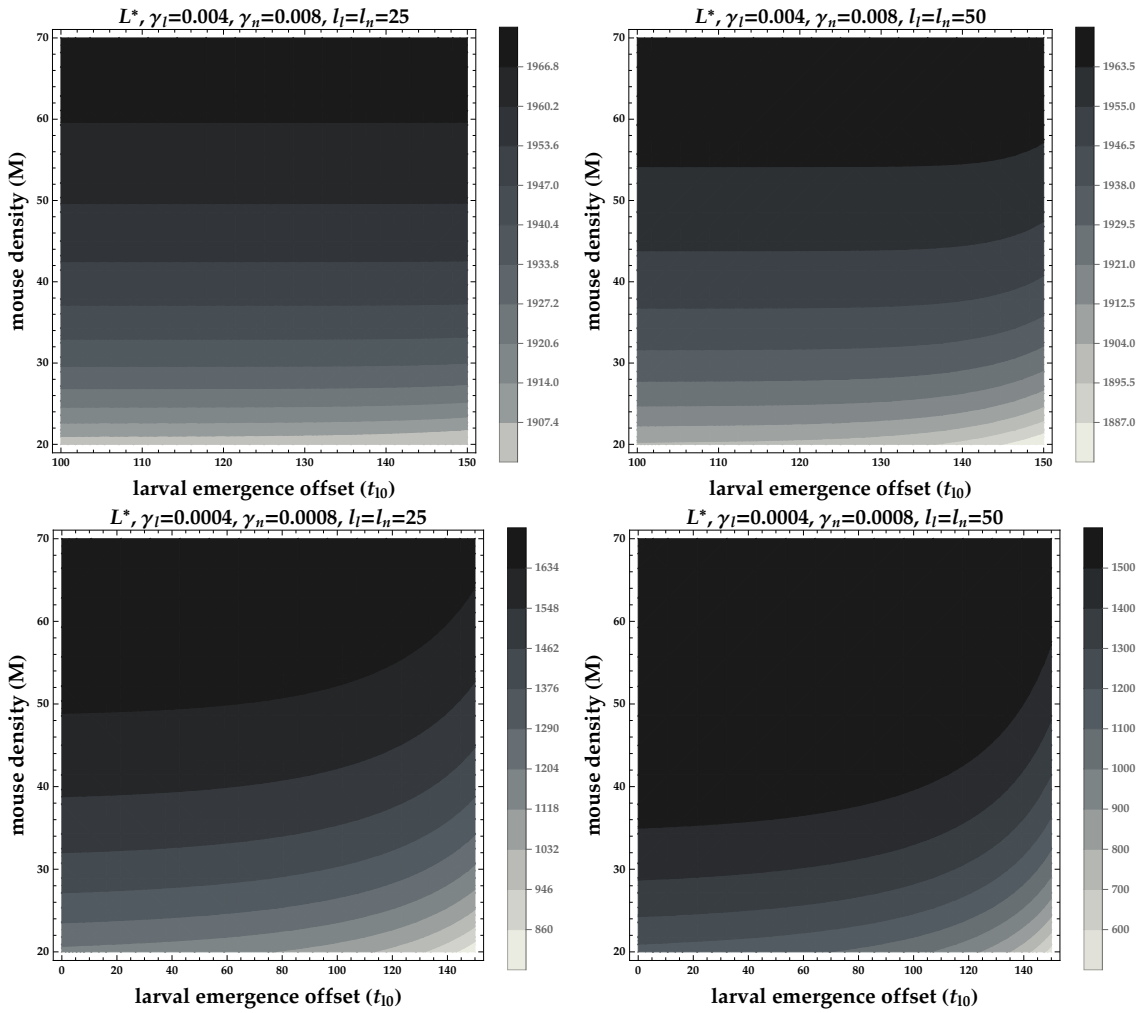

Figure A-1: Equilibrium larval population sizes ($\hat{L}^*$) decrease for highly asynchrounous nymphal and larval activity and low mouse density. $M = k(1 - \mu_m/b)$ is the mouse population size, t_{l0} is the offset between when nymphs and larvae begin emerging, γ_l and γ_n are the contact rates between larvae and mice and nymphs and mice respectively. The first row shows that if γ_l and γ_n are high, large t_{l0} decreases $\hat{L}^*$ slightly when nymphal and larval emergence is broad (l_l and l_n). The second row shows that if γ_l and γ_n are low, large t_{l0} decreases $\hat{L}^*$ more strongly, especially when nymphal and larval emergence is broad (l_l and l_n). Note that contour colors are not the same across plots. All other parameter values are shown in Table 1.

assumed for all phenological patterns.

$$R_{0nc} = \sigma_l \phi_{li}(\hat{N}_i)\hat{L}$$

where R_{0nc} refers to the fact that R_0 is "not corrected."

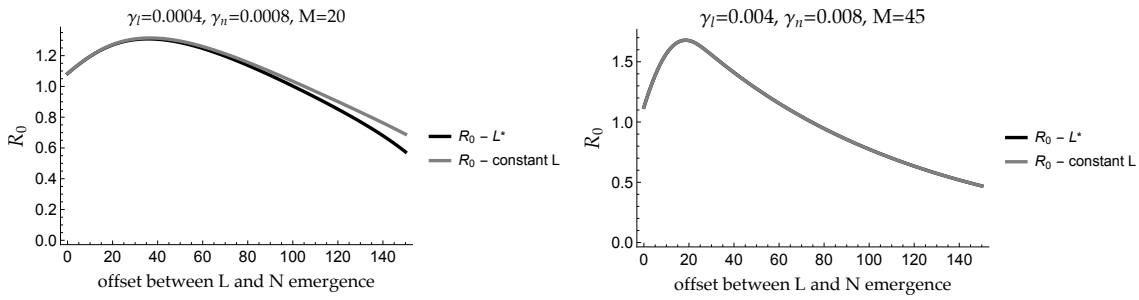

Figure A-2: The difference between R_0 that takes into account $\hat{L}^*$ (blue line) and R_{0nc} that assumes constant $\hat{L}$ irregardless of phenology (yellow line) is most dramatic for large offset between nymphal and larval activity, low contact rates between ticks and mice ($\gamma_l = 0.0004, \gamma_n = 0.0008$) and low mouse density ($M = 20$). The difference between R_0 and R_{0nc} is negligible for higher contact rates ($\gamma_l = 0.004, \gamma_n = 0.008$) and higher mouse density ($M = 45$). $\hat{L}$ was calculated using the equation (A.3) for $\hat{L}^*$ when nymphal and larval phenology is synchronous ($t_{l0} = 0$). As the offset between nymphal and larval activity increases, $\hat{L}^*$ and $\hat{L}$ diverge driving differences in estimates for R_0 and R_0nc.

The relative error between R_0 and R_{0nc} is calculated as $\frac{R_{0nc}-R_0}{R_0}$.

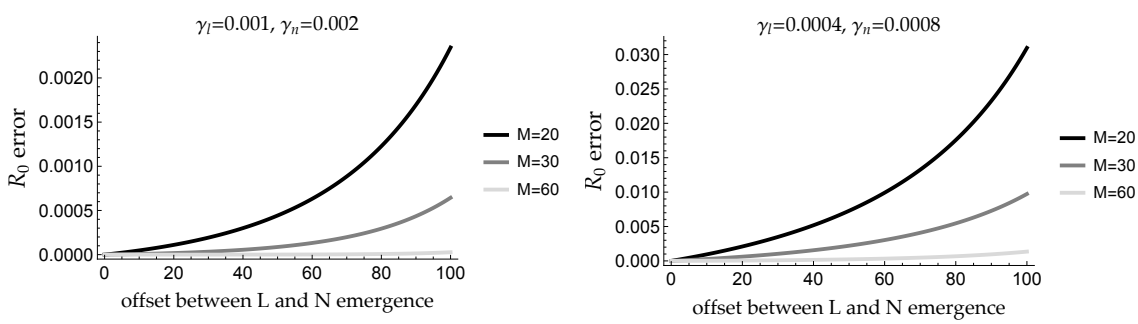

Figure A-3: The relative error between R_0 and R_{0nc} increases as the offset between larval and nymphal emergence increases. This error is exacerbated for low host density and low contact rates between ticks and mice because fewer ticks successfully feed by the end of the season which drives lower equilibrium tick sizes. $M = k(1 - \mu_m/b)$ is the mouse population size, γ_l and γ_n are the contact rates between larvae and mice and nymphs and mice respectively. All other parameter values are shown in Table 1.

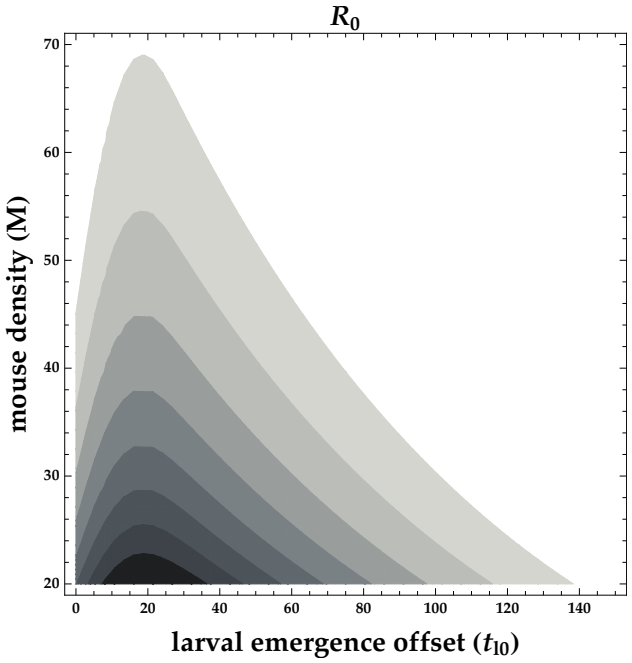

Figure A-4: R_0 decreases as mouse density increases because of dilution. R_0 decreases for highly asynchrounous nymphal and larval activity because of mouse turnover.